Journal of Power Sources 189 (2009) 309–314

Contents lists available at ScienceDirect

Journal of Power Sources

journal homepage: www.elsevier.com/locate/jpowsour

Effects of heteroatoms and nanosize on tin-based electrodes

Ricardo Alcántara, Gregorio Ortiz, Inés Rodríguez, José L. Tirado*

Laboratorio de Química Inorgánica, Universidad de Córdoba, Edificio C3, Campus de Rabanales, 14071 Córdoba, Spain

ARTICLE INFO

Article history:
Received 17 June 2008
Received in revised form 14 August 2008
Accepted 8 September 2008
Available online 18 September 2008

Keywords:
Intermetallics
Lithium batteries
^{119}Sn Mössbauer
Nanostructure

ABSTRACT

Tin-based intermetallic compounds of different compositions and with micro and nano-sized particles are studied as electrodes for lithium ion batteries. Crystalline microsized particles of $CoSn_x$ are obtained at high temperatures, while crystalline nano-sized particles are obtained at low-temperature following a one-pot method which is based on TEG solvent and reduction with $NaBH_4$. The observed capacities of $CoSn_x$ compounds in lithium test cells depend on the tin content, electrochemical cycling conditions and crystallite size. The change of the ^{119}Sn Mössbauer isomer shift upon the electrochemical reaction with lithium is more limited for the intermetallic compounds $CoSn_x$ than for pure Sn. Nano-sized $CoSn_x$ materials show superior specific capacity than microsized $CoSn_x$ powders. The maximum observed reversible capacity of nano-Co_3Sn_2 is equal to 544 m Ah g^{-1} in the first cycle, while 413 m Ah g^{-1} were observed for nano-CoSn.

© 2008 Elsevier B.V. All rights reserved.

1. Introduction

Because of its ability to form intermetallic compounds with lithium, from time ago there has been a great interest in the potential use of tin as electrode active material for lithium ion batteries. Mainly due to marked volume changes, the initial high capacity of pure tin to react with lithium becomes impractical after prolonged cycling. The two main strategies to overcome electrode failure are: (i) adding heteroelements (e.g. 3d elements and carbon) and (ii) amorphization, nanosizing and nanoshaping of the intermetallic particles [1–7]. These two aspects are studied in this work.

A nanostructured intermetallic compound with a great relative amount of tin that holds the nano-sized character upon successive charge–discharge cycles would be an excellent electrode. ^{119}Sn Mössbauer spectroscopy is used here as a tool to unfold the interactions of tin atoms with heteroelements. Since $CoSn_x$ compositions show a great ability to form amorphous alloys with a relatively high energy of crystallization [8], these are particularly promising for our purposes.

2. Experimental

Micro-$CoSn_x$ compounds were prepared by annealing mixtures of metallic Co and Sn in the adequate relative amounts under an argon flow at the desired temperature (over 300 °C), as described in elsewhere [1,2,6]. Typically, single-phase micro-CoSn was obtained at 500 °C.

Nano-$CoSn_x$ compounds were prepared by dissolving anhydrous $SnCl_2$ and $Co(COOCH_3)_2 4H_2O$ in tetraethyleneglycol (TEG) in the desired atomic ratio, dispersing polyvinylpyrrolidone (PVP, MW = 40,000) and adding $NaBH_4$, with a strict control over the atmosphere (Ar-flow) and the temperature. The procedure is based on a previously described one-pot method [2,6]. The volume of the reactor vessel was 1 L. The preparation of nano-CoSn was achieved only in the very small scale, typically using 100 mL of TEG and 265 °C. Nano-Co_3Sn_2 was obtained at the same temperature and using 300 mL of TEG.

X-ray diffraction (XRD) diagrams were recorded on a Siemens D5000 instrument and using Cu Kα radiation. The crystallite size was calculated using the Scherrer equation and using LaB_6 was used as a reference material for linewidth correction. Transmission electron microscopy (TEM) images were obtained with a JEM-2010 apparatus. The ^{119}Sn Mössbauer spectra were recorded in the transmission geometry at room temperature by using and a $Ba^{119}SnO_3$ source. The ^{119}Sn isomer shifts are referenced to $BaSnO_3$ (δ = 0.0 mm s^{-1}).

The electrochemical experiments were carried out in a MacPile instrument, using Swagelok-type cells, and $LiPF_6$ in an EC:DEC solvents mixture as electrolytic solution. The negative electrode was a piece of Li, while the positive electrode was constituted by active material ($CoSn_x$, 87 wt.%), carbon (graphite Super-P, 8 wt.%) and binder (PVDF, 5 wt.%). Alternative values were active material ($CoSn_x$, 77 wt.%), carbon (carbon black + graphite, 15 wt.%) and binder (PVDF, 8 wt.%) were used in the composite electrode.

* Corresponding author. Tel.: +34 957218637; fax: +34 957218621.
E-mail address: iq1ticoj@uco.es (J.L. Tirado).

0378-7753/$ – see front matter © 2008 Elsevier B.V. All rights reserved.
doi:10.1016/j.jpowsour.2008.09.013

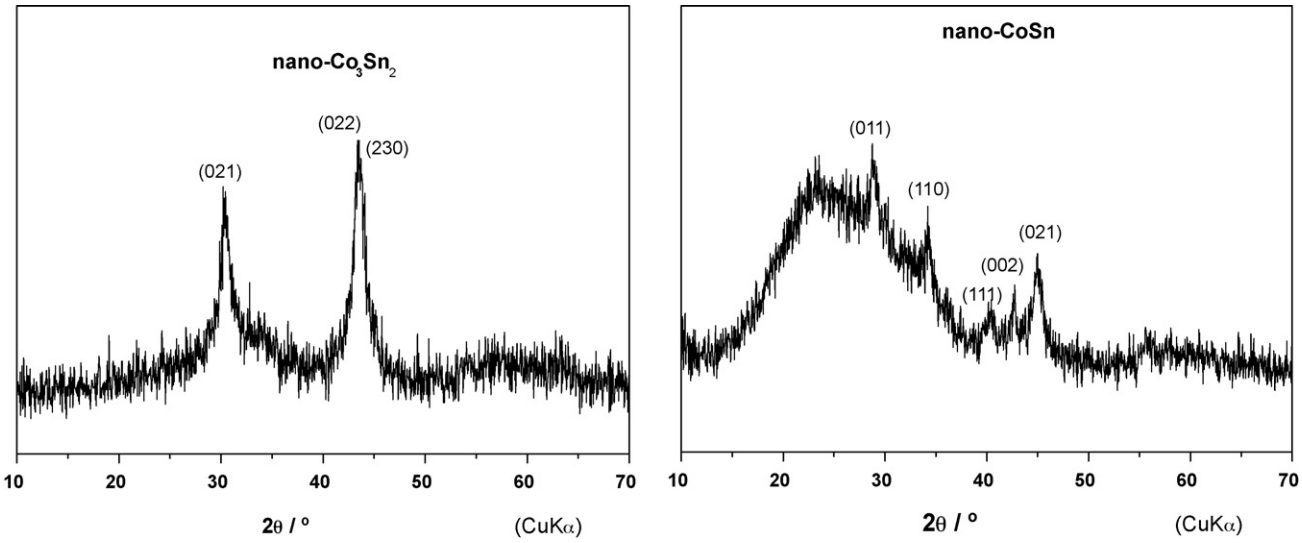

Fig. 1. XRD of nano-Co_3Sn_2 and nano-CoSn.

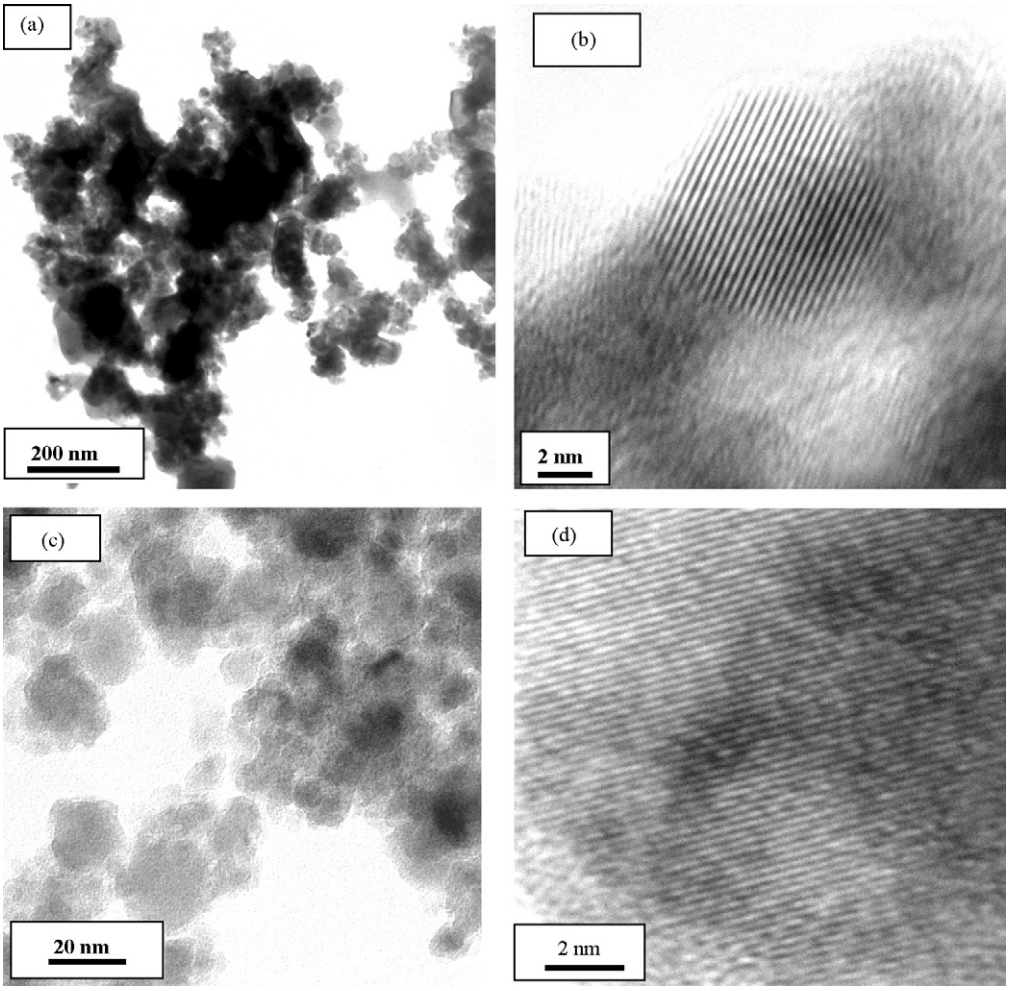

Fig. 2. TEM micrographs of nano-CoSn (a and b) and nano-Co_3Sn_2 (c and d).

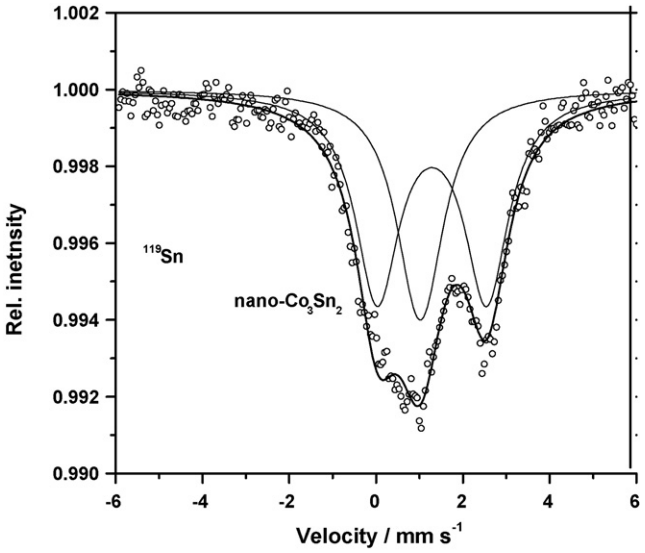

Fig. 3. ^{119}Sn Mössbauer spectrum (symbols) and fitting (lines) for nano-Co_3Sn_2.

3. Results and discussion

3.1. Preparation and characterization of micro- and nano-$CoSn_x$

The high-temperature synthesis in a furnace of cobalt–tin intermetallics ($CoSn_x$) starting from the elements leads to micrometric-sized particles (micro-$CoSn_x$) and ill-defined morphologies. The occurrence of envelops of different compositions surrounding the core of the particle, as due to peritectic reactions, is a usual feature. This is also valid for the tin-flux method that uses a tin excess (e.g. Co:Sn atomic ratio equal to 1:4) [1,9]. However, submicrometric particles of controlled morphologies can be advantageous for the electrochemical performance [6]. The low-temperature synthesis based on TEG solvent and chemical reduction of the ions with boronhydride in the presence of polymers allows controlling particle size in the nanometric range and particle morphology, thus tailoring texture and microstructure in the final nano-$CoSn_x$ compound.

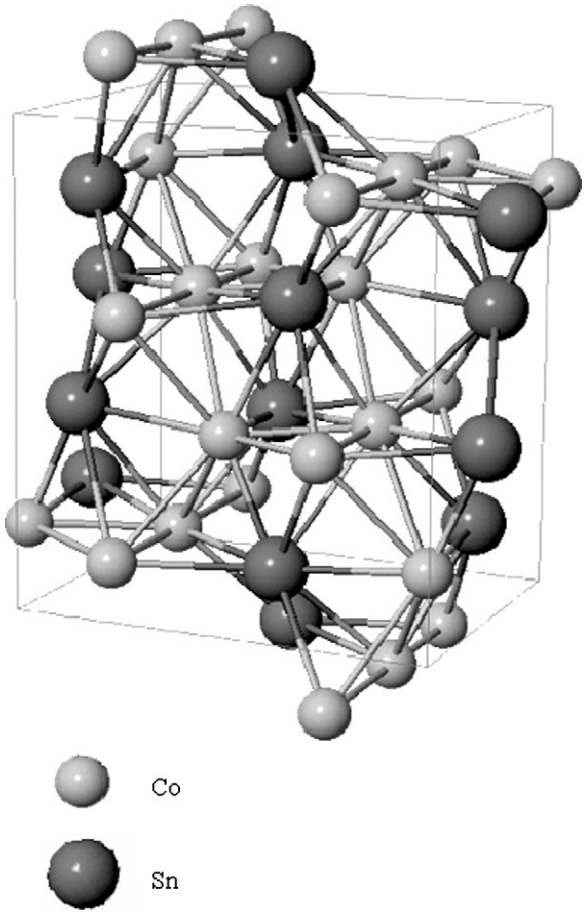

Fig. 4. Crystal structure of orthorhombic Co_3Sn_2. The larger spheres represent tin atoms and the smaller spheres represent cobalt atoms.

Table 1
^{119}Sn Mössbauer parameters for the fitting of the spectrum corresponding to nano-Co_3Sn_2.

δ	Δ	Γ	C
1.012(6)	0.2(1)	1.22(4)	37
1.29(2)	2.52(3)	1.22(5)	63

δ: isomer shift (mm s^{-1}). Δ: quadrupole splitting (mm s^{-1}). Γ: line width (mm s^{-1}). C: relative contribution (%).

XRD patterns and TEM micrographs of the obtained nanocrystalline intermetallics with compositions CoSn and Co_3Sn_2 are shown in Figs. 1 and 2, respectively. The XRD pattern of nano-CoSn can be indexed in hexagonal lattice, according to space group *P6/mmm* (PDF card number 2-559). The XRD-pattern of nano-Co_3Sn_2 agrees well with the Powder Diffraction File number 27-1124. Impurity phases are not detected. The average crystallite size values calculated from the linewidth of the XRD reflections were 8 and 23 nm, for nano-CoSn and nano-Co_3Sn_2, respectively. The lattice fringes that are observed in the TEM micrographs in Fig. 2 corroborate the crystalline structure of the samples irrespective of the nanometric grain size. The particles of nano-CoSn tend to form fibrous aggregates.

3.2. ^{119}Sn Mössbauer spectroscopy: the role of heteroelements

^{119}Sn Mössbauer spectroscopy gives information on the 5s electron density at the absorber tin nuclei. This can be used for the

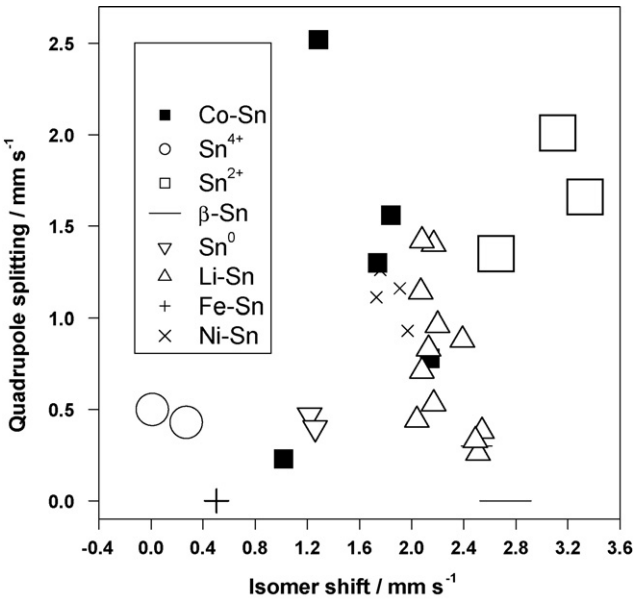

Fig. 5. Quadrupole splitting and isomer shift values for ^{119}Sn Mössbauer spectra of tin-containing compounds. Data are also taken from the literature.

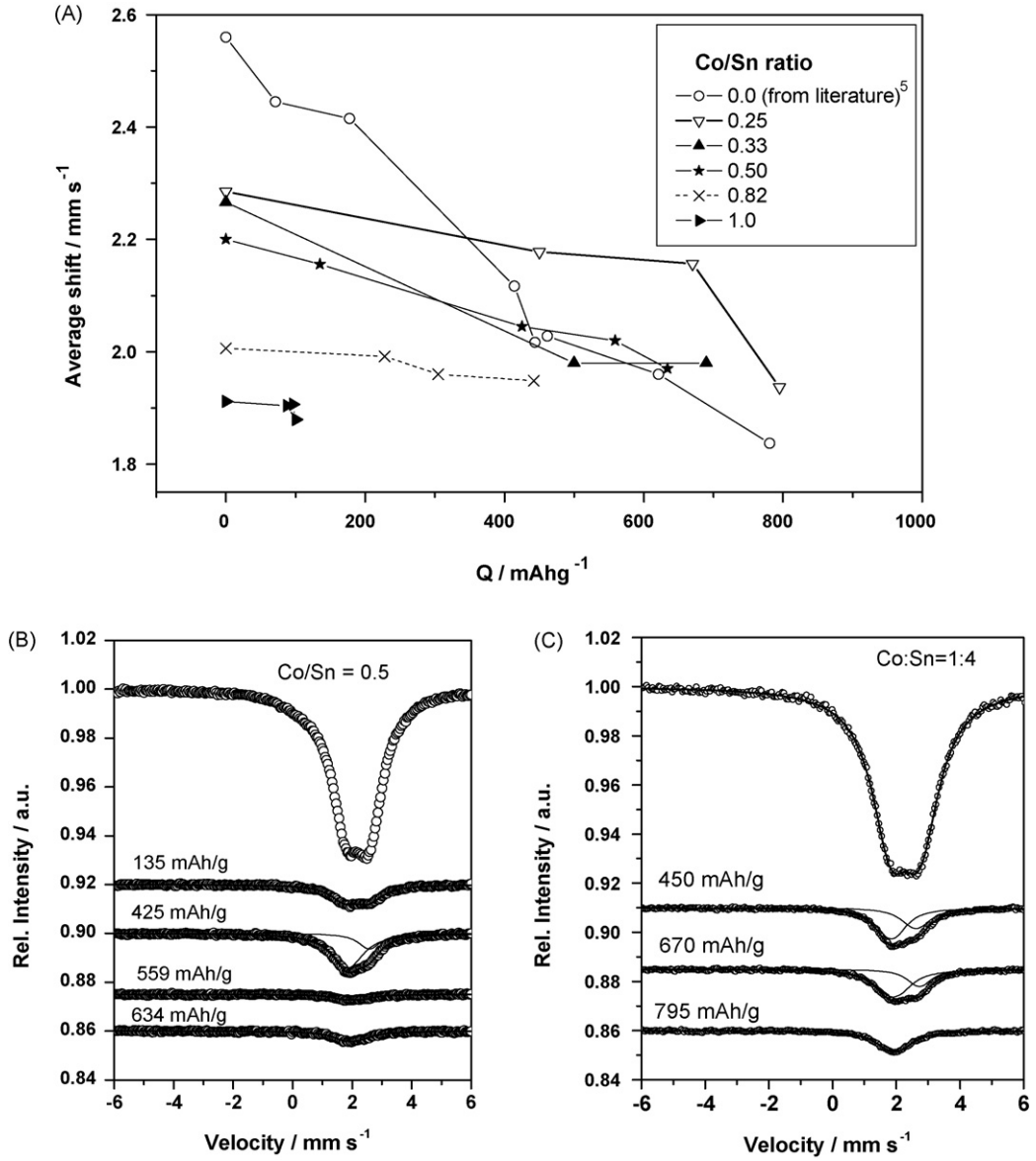

Fig. 6. ^{119}Sn Mössbauer spectroscopy results for micro-$CoSn_x$ intermetallics with different nominal Co/Sn atomic ratios. (a) Average ^{119}Sn isomer shift and as a function of the discharge depth in lithium cells. (b) Spectra for Co/Sn = 0.5 after reaction with lithium. (c) Spectra for Co/Sn = 0.25 after reaction with lithium.

characterization of intermetallics. The ^{119}Sn Mössbauer spectrum of nano-CoSn has been published in elsewhere [6]. The spectrum of nano-Co_3Sn_2 is shown in Fig. 3. The experimental spectrum cannot be fitted with only one signal. According to the diffractions studies and structural refinement reported by Fjellvag and Kjekshus, there are two different 4c (x, 1/4, z) sets of four crystallographically equivalent tin atoms each in Co_3Sn_2 with NiAs-derived atomic arrangement and space group *Pnma* [10] (Fig. 4). One of them includes tin atoms with Sn–Sn bonds. Thus, the spectrum can be fitted with two doublet signals with different isomer shift and quadrupole splitting and the same linewidth (imposed condition) and the results are shown in Table 1.

The average isomer shifts of the ^{119}Sn Mössbauer spectra are shifted from $\delta = 2.6\,mm\,s^{-1}$ for pure tin, to lower values (until ca. $1.9\,mm\,s^{-1}$) for $CoSn_x$ compounds (Figs. 5 and 6). The same tendency to decrease the ^{119}Sn isomer shift value is observed for nickel and iron intermetallics. In contrast, the addition of carbon atoms tends to slightly increase the isomer shift of the Co–Sn phases [1]. These features can be related to the relative values of electronegativity for carbon, cobalt, iron and tin atoms. The isomer shift values of $CoSn_x$ and $NiSn_x$ fall in the same range ($2.5–1.7\,mm\,s^{-1}$) than that of Li_xSn. The quadrupole splitting is affected by the higher or lower symmetry that surrounds the tin atoms. Nanocrystalline intermetallics can exhibit lower tin recoil-free fraction than microcrystalline intermetallics, and the resulting low intensity of the spectra can make the analysis more difficult [2]. The interpretation of the ^{119}Sn Mössbauer spectra for Li_yCoSn_x phases is not evident. Nabli et al. found a short-range order in amorphous $CoSn_x$ alloys and the ^{119}Sn Mössbauer spectra were fitted with broad assymetrical doublets representing environments close to that of tin in crystalline CoSn [11]. Our spectra can be fitted using one or several doublets, and each of them do not represent necessarily a unique tin site. According to the XRD diagrams and the ^{119}Sn Mössbauer spectra, unknown amorphous Li_yCoSn_x phases seem to be formed, that can be also regarded as metallic glasses. It can be observed in Fig. 6 that the incorporation of lithium into all the studied tin-based phases decreases the average isomer shift (barycentre of the whole spectrum). This can be explained as due to a higher electron

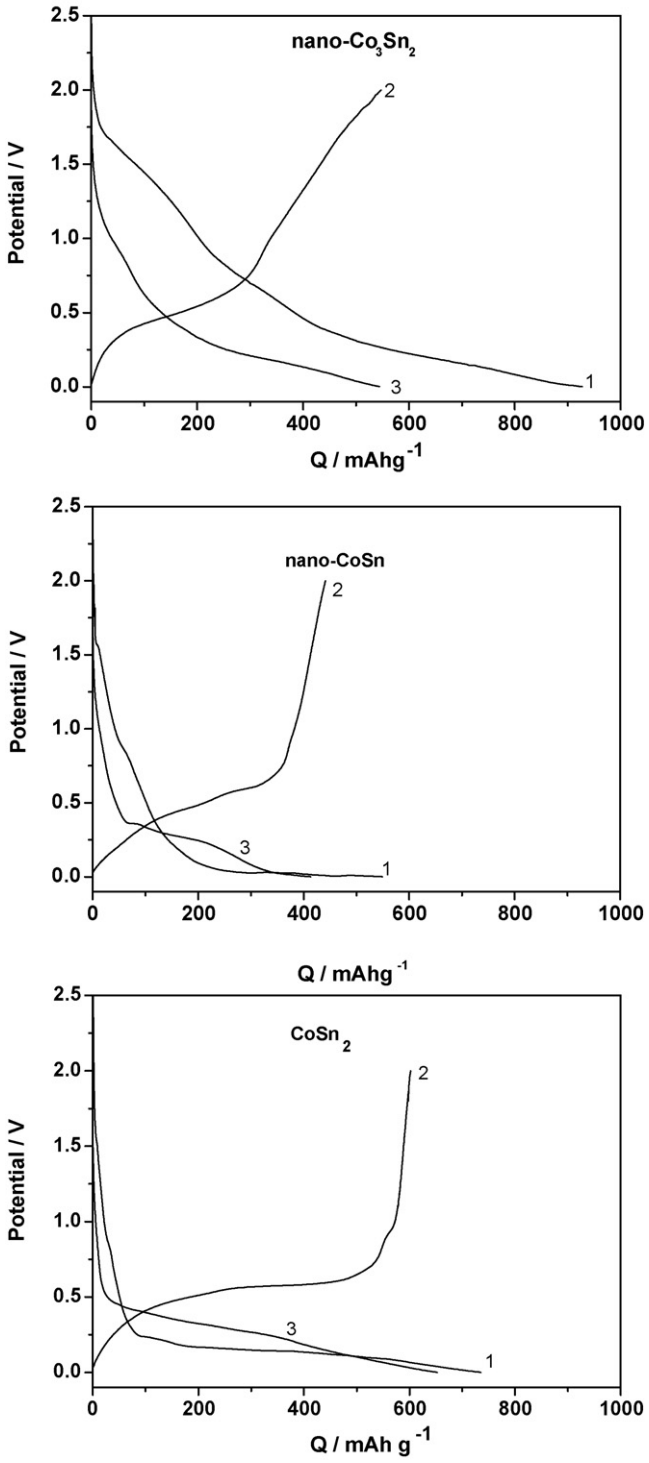

Fig. 7. Potential–capacity curves for nano-Co_3Sn_2, nano-CoSn and micro-$CoSn_2$ intermetallic compounds in lithium test cells. Current density was 10 mA g^{-1} for both charge and discharge. The successive discharge and charge branches are numbered (1–3).

density at the tin sites after reaction with lithium, or as due to the decrease in the number of tin–tin interactions that are disrupted by lithium atoms. It is worth to note that the range of this isomer shift change upon reaction with lithium is more limited for $CoSn_x$ intermetallics than pure Sn. Otherwise, the cobalt d-electrons contribution can largely contribute to the stability of the amorphous $CoSn_x$ alloys and avoid crystallization processes [8]. These features

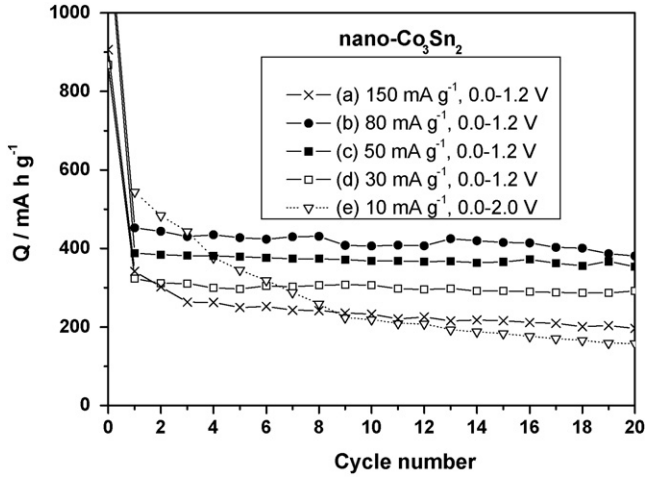

Fig. 8. Specific capacities of nano-Co_3Sn_2 in lithium test cells at different current intensities and voltage limits. 77 wt.% of active material is used in (a–c), while 87 wt.% is used in (d).

can contribute to the stabilization of the electrode upon cycling, avoiding abrupt changes and finally the battery failure.

3.3. Electrochemistry of $CoSn_x$

The electrochemical results of the different samples studied here and in previous reports [1,2,6] show that the capacities of the $CoSn_x$ compounds in lithium test cells depend on tin content, crystallite size and electrochemical cycling conditions. For a same composition, the nano-$CoSn_x$ compounds usually exhibit higher capacities but poorer capacity retention in comparison with micro-$CoSn_x$. Thus, it was reported that the reversible capacity of micro-CoSn is below 100 mAh g^{-1} [6]. The reversible capacity for nano-CoSn achieved here is equals to 413 mAh g^{-1} (Fig. 7). Xie et al. found that the first capacity of amorphous Co_3Sn_2 obtained by solvothermal route is equals to 363 mAh g^{-1}, while the capacity of crystalline Co_3Sn_2 is below 100 mAh g^{-1} [12,13]. The observed maximum reversible capacity of nano-Co_3Sn_2 was 544 m Ah g^{-1} (Fig. 8), which is nearly the theoretical maximum value. Most probably, the slow diffusion of lithium in the outer layers of the coarse particles is the limiting-factor for the micro-$CoSn_x$ phases, while the grains that do not react with Li can stabilize the electrode. To avoid problems with side reactions and to allow percolation, the optimization of the electrolytic solution and binder is fundamental for the future improvement of the electrochemical performance of nano-$CoSn_x$ upon prolonged cycling. The mechanical properties are another key factor for improving the cyclability of the electrodes [14]. The capacity retention upon cycling of nano-Co_3Sn_2 is improved by selecting the electrode additives and cycling conditions (Fig. 8). Using composite electrodes containing 77% of active material and cycling between 0.0 and 1.2 V, the specific capacity increases when the current density is increased from 30 to 80 mA g^{-1} (Fig. 8a–c). This behavior is unusual. We have observed that much current density (150 mA g^{-1}) yields to lower capacity in nanocrystalline Co_3Sn_2. Using a composite electrode containing 87% of active material and cycling at very low current density (10 mA g^{-1}) with potential limits of 0.0–2.0 V, the capacity observed in the first cycles is higher (Fig. 8d). The capacity retention after a few cycles is lower at the lowest current density (Fig. 8d), probably due to irreversible electrolyte consumption at slow kinetics and/or the volume changes of the active material that are not buffered by the electrode additives. Xie et al. showed that amorphous Co_3Sn_2 undergoes a crystallization process during cycling that leads to capacity fading [12].

Probably, the selected kinetics (10–80 mA g^{-1}) also can influence on the crystallization process of the active material that is generated after the reaction of lithium with nanocrystalline Co_3Sn_2. Capacities over 400 m Ah g^{-1} after 10 cycles are observed for the electrode with 77 wt.% of active material and 0.0–1.2 V of potential limits.

In summary, nanocrystalline $CoSn_x$ phases are particularly promising as electrode active material and exhibit electrochemical behavior superior to microcrystalline $CoSn_x$ phases. It seems that the nanometric size of the grains (as is deduced from XRD and TEM) makes easier a rapid and extended reaction with lithium, and the cobalt atoms help to stabilize the resulting Li_yCoSn_x metallic glass (as is deduced from ^{119}Sn Mössbauer spectra). Thus XRD, TEM and ^{119}Sn Mössbauer spectroscopy studies on nanocrystalline $CoSn_3$ let us to confirm that the nanocrystalline character yields to high specific capacities values, and the presence of cobalt atoms can avoid the formation of crystalline phases upon cycling, as is reported elsewhere [15]. However, further studies are needed to completely understand the reaction mechanisms of the $CoSn_x$ phases.

4. Conclusions

After the reaction of the tin-based electrodes with Li, the presence of cobalt atoms helps to the formation of relatively stable amorphous intermetallic phases. Nanocrystalline $CoSn_x$ compounds can show superior electrochemical performance than microcrystalline $CoSn_x$ compounds. Nanocrystalline Co_3Sn_2 shows reversible capacities over 400 m Ah g^{-1} after several cycles.

Acknowledgments

The authors are indebted to MEC (MAT2005-00374), SCAI-UCO and *Junta de Andalucía* (research group FQM288). RA is indebted to MEC (CTQ2008-03192).

References

[1] G.F. Ortiz, R. Alcántara, I. Rodríguez, J.L. Tirado, J. Electroanal. Chem. 605 (2007) 98.
[2] R. Alcántara, P. Lavela, G. Ortiz, J.L. Tirado, Hyperfine Int., doi:10.1007/s10751-008-9866-7.
[3] P.P. Ferguson, A.D.W. Todd, J.R. Dahn, Electrochem. Commun. 10 (2008) 25.
[4] C.M. Ionica-Bousquet, P.E. Lippens, L. Aldon, J. Olivier-Forucade, J.C. Jumas, Chem. Mater. 18 (2006) 6442.
[5] R.A. Dunlap, R.A. Small, D.D. MacNeil, M.N. Obrovac, J.R. Dahn, J. Alloys Compd. 289 (1999) 135.
[6] R. Alcántara, I. Rodríguez, J.L. Tirado, Chem. Phys. Chem. 9 (2008) 1171.
[7] J. Hassoun, G. Mulas, S. Panero, B. Scrosati, Electrochem. Commun. 9 (2007) 2075.
[8] J.G. Geny, D. Malterre, M. Vergnat, M. Piecuch, G. Marchal, J. Non-Cryst. Solids 62 (1984) 1243.
[9] M.G. Kanatzidis, R. Pöttgen, W. Jeitschko, Angew. Chem. Int. Ed. 44 (2005) 6996.
[10] H. Fjellvag, A. Kjekshus, Acta Chem. Scand. A 40 (1986) 23.
[11] N. Nabli, M. Piecuch, J. Durand, G. Marchal, P. Delcroix, Hyperfine Int. 27 (1986) 321.
[12] J. Xie, X.B. Zhao, G.S. Cao, J.P. Tu, J. Power Sources 164 (2007) 386.
[13] J.R. Dahn, R.E. Mar, A. Abouzeid, J. Electrochem. Soc. 153 (2006) A361.
[14] N. Tamura, M. Fujimoto, M. Kamino, S. Fujitano, Electrochim. Acta 49 (2004) 1949.
[15] R. Alcántara, U. Nwokeke, I. Rodríguez, J.L. Tirado, Electrochem. Solid-State Lett. 11 (2008) A209.